

Climatology of water excesses and shortages in the La Plata Basin

Carlos M. Krepper · Graciela V. Zucarelli

Received: 3 December 2007 / Accepted: 3 November 2009 / Published online: 15 December 2009
© Springer-Verlag 2009

Abstract This study presents a multitemporal climatology of water excess and shortage during the 20th century in the La Plata Basin. The climatology is based on $0.5^\circ \times 0.5^\circ$ grid across the region. We transform monthly precipitation series for each point into index series at different time scales using the Standardized Precipitation Index (SPI). A month is under water excess (shortage) conditions at different time scales ($i=6, 9, 12,$ and 18 months), when $SPI[i](j) > 1.5$ ($SPI[i](j) < -1.5$), where j is the current month. Trends in precipitation were determined using mean regional series of average values over the entire basin. A month when more than 30% of the total basin is under water excesses (shortages) is defined as an excess (shortage) critical month. From the vulnerability point of view, we analyzed the occurrence of critical months. The number of excess critical months increase with time scale of index, and almost all the critical months occurred after 1950 as a consequence of the low-frequency precipitation pattern. That means a noticeable increase in the vulnerability to extended excesses (more than 30% of the area under water excesses) after 1950, especially over the Upper Paraná and the Uruguay basins. For shortage critical months, the behavior depends on time scales. At large time scale (18 and 12 months), almost all the shortage critical months occurred in the period 1901–1950 and only at shorter time scale (9 and 6 months), some critical months appeared after 1950. That means a noteworthy

decrease in the basin vulnerability to extended water shortage after 1950 and a moderate decrease in vulnerability to generalized shortage. If we analyze the frequency and mean duration of water excess and shortage events across the basin, we can appreciate that there is a tendency to relate higher frequency regions with regions with lower mean duration events, and conversely.

1 Introduction

The La Plata Basin is one of the largest in the world; it extends over an area of approximately 3,100,000 km² and covers territories in five countries, namely Argentina, Bolivia, Brazil, Paraguay, and Uruguay (Fig. 1). The total population of the basin amounts to more than 100 million inhabitants, 87% of which live in urban areas (UNESCO-WWAP 2007). This basin has an enormous economic and social importance since there you can find forty main cities (with more than 100,000 inhabitants), including five capital cities, seventy-five large dams, and an economy that represents 70% of the gross national product of the five countries combined (Tucci 2001; UNESCO-WWAP 2007). The main portion of this large drainage area is in the southern part of Brazil where it covers 1,415,000 km²; with 920,000 km² in Argentina; 410,000 km² in Paraguay; 205,000 km² in Bolivia; and a large part of Uruguay with 150,000 km² (Garcia and Vargas 1996). However, despite its extensive geographical distribution, more than 70% of the water that flows in the main rivers comes from rain that falls in Brazil. A third of the total basin barely contributes with only 500 m³ s⁻¹ of a total of over 22,000 m³ s⁻¹ (Garcia and Vargas 1998).

Within the La Plata Basin, four large hydrographic units can be differentiated: the Paraná River, the Paraguay River,

C. M. Krepper (✉)
CONICET–Facultad de Ingeniería y Ciencias Hídricas,
Universidad Nacional del Litoral,
Santa Fe, Argentina
e-mail: ckrepper@fich1.unl.edu.ar

G. V. Zucarelli
Facultad de Ingeniería y Ciencias Hídricas,
Universidad Nacional del Litoral,
Santa Fe, Argentina

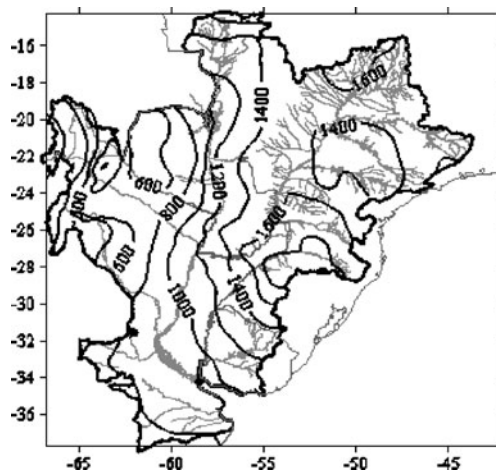


Fig. 1 Annual mean precipitation (mm) for the period 1901–2000

the Uruguay River, and the La Plata system itself (Garcia and Vargas 1996, 1998). The Paraná and the Uruguay Rivers constitute the Río de la Plata River, while the Paraguay River flows directly into the Paraná River, a few kilometers upstream from Corrientes City.

An interesting point concerns the relative flow contribution of major rivers in the basin. Table 1 presents the annual mean flows at selected stations, the corresponding drainage area, and the specific runoff (runoff per unit drainage area). The basic data were obtained from Garcia and Vargas (1998) for the period 1931–1992. In Table 1, we can appreciate that larger specific runoff ($l\ km^{-2}\ s^{-1}$) correspond to the Uruguay River and the lower, to the Paraguay River. The Paraná River is the most important tributary of the Río de la Plata and contributes with approximately 78% to the Rio de la Plata flow.

The water resources sustain one of the most productive regions where the main economic activities are cereal production and cattle-raising.

The austral summer circulation over South America is dominated by the South America Monsoon System (SAMS). Zhou and Lau (1998) have demonstrated that the summer season circulation in South America contains the essential ingredients to be characterized as a monsoon system. These authors identified five different phases in the time evolution of the SAMS from August 1989 to April 1990. This period correspond to a typical normal year (near normal tropical Sea Surface Temperature, SST), when the influence of interannual variability is relatively small. In the premonsoon phase, a center of the upper-level divergence and the lower level convergence are located above the Amazon basin. During the development phase, a low-level cyclonic activity arises to the southeast of Altiplano (the Chaco low). Meanwhile, the equatorial trade winds cross the equator and the Andes block and deflect the flow into

the Chaco low. The moisture transport intensifies locally along the eastern flank of the Andes and the subtropical South Atlantic High (SAH) moves towards the continent carrying water vapor from the South Atlantic Ocean into subtropical South America. The South American low-level jet (SALLJ) is embedded in the low-level southward flow, east of the Andes and is present throughout the year (Berbery and Barros 2002). This climatological feature is particularly stronger during the summer season and links the tropics with subtropical plains and La Plata Basin. The rainfall increases over central Andes and a severe convective activity is initiated along a southeastward band extending from southern Amazon region toward southeastern Brazil and surrounding Atlantic Ocean. This convection band is known as the South Atlantic convergence zone (SACZ). When the SAMS enters in the mature phase the upper-level circulation includes a large anticyclonic circulation (the Bolivian High) near $15^{\circ}S$, $65^{\circ}W$ and an upper-level trough near the coast of northeast Brazil (Vera et al. 2006). The Chaco low together with the Bolivian High can be considered as the regional response of the tropospheric circulation to the strong convective heating over Amazon basin and central Brazil. In this stage, the heavy rainfall zone extends over the Altiplano Plateau and the southernmost subtropical plains (Nogues-Paegle and Vera 2009). During the withdrawal phase, the cross-equatorial flows weaken, and due to the reduction of moisture supply to the subtropics, the heavy rainfall zone retreats northeastward from the subtropics (Zhou and Lau 1998). In the postmonsoon phase, the rainfall returns to the tropics.

Previous studies have considered five factors for the interannual variability of precipitation associated to SAMS (Vera et al. 2006): SST anomalies, lad surface conditions, and the position and strength of tropical convergences (the Intertropical Convergence Zone (ITCZ) and SACZ), water vapor transport, and large-scale circulation. Labraga et al. (2000) describe the relative importance of local evaporation rate and the stationary and transient water vapor flux in the spatial distribution of mean seasonal precipitation rate over South America. SALLJ is a key feature of the regional

Table 1 Selected stations

River/station	Drainage area (km ²)	Mean annual discharge (m ³ s ⁻¹)	Specific runoff (lkm ⁻² s ⁻¹)
Paraná/Guairá	802,850	9,209	11.5
Paraná/Posadas	993,360	12,179	12.3
Paraná/Corrientes	2,051,720	17,037	8.3
Paraguay/Pto. Bermejo	1,095,000	3,893	3.5
Uruguay/Santo Tomé	123,120	2,468	20.0
Uruguay/Monte Caseros	217,360	4,558	21.0

climate, transporting moisture from the Amazon to the La Plata basin and this southward moisture penetration is strongly modulated on different time scales, ranging from diurnal to interdecadal periods (Vera et al. 2006). In general, floods and droughts over the basin are correlated with the intensity and position of SALLJ. The southward SALLJ episodes characterized by their farther south extension, denoted as Chaco jet events (CJEs; Salio et al. 2002; Nicolini et al. 2002), enhance precipitation over northeastern Argentina, northern Uruguay, eastern Paraguay, and southern Brazil. Although CJEs are relatively infrequent during summer season (only 17% of the summer days), they account for an important fraction of seasonal precipitation over the region (up to a maximum of 55% in some areas; Nicolini et al. 2002).

Using a general circulation model, Lenters and Cook (1995) showed that precipitation in the SACZ is enhanced by the convergence of northerly winds along the western flank of the SAH and the continental eastward branch of low-level flow from the continental low latitudes.

In the region, several authors analyzed the interannual response of precipitation to El Niño/La Niña events or directly to SST in the Pacific or Atlantic Oceans (Pisciottano et al. 1994; Nogués-Paegle and Mo 1997; Diaz et al. 1998; Grimm et al. 1998, 2000; Barros and Silvestri 2002). They concluded that El Niño-Southern Oscillation (ENSO) was responsible for most of the interannual variability during the summer season. Nevertheless, during the last decades under non-ENSO years, central-east Argentina experienced severe drought and wet conditions (Scian et al. 2006).

Doyle and Barros (2002) explore the possible links between the interannual variability of low-level tropospheric circulation and precipitation in subtropical South America with the SST in the western subtropical South Atlantic. They present a description of mean precipitation and moisture transport throughout the year and found a qualitative agreement between precipitation and the low-level water vapor transport fields. These authors show that the SST interannual variability in the western subtropical South Atlantic is related to the summer low-level flow and anomalies of precipitation in subtropical South America. During warm conditions of the subtropical South Atlantic, there are two maxima of precipitation, one in the continental extension of the southward-displaced SACZ and the other centered in north eastern Argentina and southern Brazil. Under cold conditions of the subtropical South Atlantic, the positive anomalies of precipitation are in the continental extension of the SACZ, which is shifted northward of its mean position, while negative anomalies of precipitation are observed in northeastern Argentina and southern Brazil (Doyle and Barros 2002). A review of the relation of the SAMS with the climate of South America south of 20°S can be found in Barros et al. (2002).

Annual mean rainfall in the La Plata Basin tends to decrease both from north to south and from east to west. The maximum annual precipitation (Fig. 1) occurs in the upper part of the Uruguay River basin (more than 1,800 mm year⁻¹) and the minimum, in the Bolivian High Plateau (less than 400 mm year⁻¹).

According to Giorgi (2002), South America is one of the regions in the world that featured large positive trend values for annual and summer precipitation in the twentieth century. Nevertheless, to the west of The Andes mountains, the precipitation trends became negative (Minetti and Vargas 1998; Berbery et al. 2006). Long-term changes in annual precipitation patterns in almost the entire southeastern South American region have been mentioned by several authors (Castañeda and Barros 1994, 2001; Minetti and Vargas 1998). Krepper and Sequeira (1998) studied the low-frequency variability of rainfall in the southern portion of the La Plata Basin. They found evidence of a sustained positive precipitation trend from the 1950 onwards. This characteristic low-frequency precipitation pattern affects an extensive area, which includes part of the northeast and center of Argentina, almost the whole of Uruguay and a very limited part of the state of Rio Grande do Sul in Brazil. Rainfall in the wet Pampa in Argentina experienced important changes in average quantity of rainfall received annually throughout the last century. In some places, said variation represented an increase of more than 50% when we compare the first decade (1901–1910) with the 1981–1988 period (Krepper and Sequeira 1998). These trends have had a considerable impact on agricultural production and on the generation of hydraulic power of the region. Over Argentina territory, the annual mean isohyets have a meridional orientation where the amount of annual rainfall decreases from east to west. Thus, the trends in precipitation have resulted in a westward shift of the isohyets and an increased in the land with aptitude for crop cultivation of around 100,000 km² (Berbery et al. 2006). Therefore, from the regional economy point of view, it is important to know whether these trends will be reverse or not in the next decades. Liebmann et al. (2004) analyzed seasonal linear trends of precipitation in South America laying emphasis on central South America. They concluded that there was a large positive trend for summer (January–March) precipitation in southern Brazil from 1976 to 1999. Said trend resulted from increases in the number of days it rained and larger amount of water fallen per event, and the authors found a good correlation between this trend and a simultaneous warming in the sea surface temperature in part of the South Atlantic Ocean.

More recently, Barros et al. (2008) have identified two independent processes related to precipitation trends observed in subtropical South America; trends in the leading modes of the Sea Surface Pressure fields during warm semester (October–March) and changes in ENSO.

Different regions in the La Plata Basin are affected by flooding, which, depending on its severity, can significantly alter regional and national economic development. Most of the rivers of the La Plata Basin have long and wide flood plains used for crop production or settlements (Tucci and Clarke 1998). Large areas of land along the Paraná margins are affected periodically by flood events, which produce considerable losses. The largest flood of the last century occurred along the Paraná River in 1983 and featured the highest monthly discharges and a one-and-a-half-year persistence from July 1982 to December 1983. During such flood, more than 100,000 people had to be evacuated and economic losses amounted to more than one billion dollars. Anderson et al. (1993) analyzed flooding in the Paraná-Paraguay basin for the period 1901–1992, and they found that flooding was both more frequent and more severe in the latter part of the period. Camilloni and Barros (2003) analyzed extreme discharge events in the Paraná River and their climate forcing. They found a clear relationship between the phases of ENSO and major discharges.

The scientific literature is plenty of drought definitions reflecting the area of interest or the purpose of study (Dracup et al. 1980). The American Meteorological Society (1997) grouped the different definitions of droughts into four basic types: meteorological or climatological, agricultural, hydrological, and socioeconomic. Meteorological or climatological drought is defined in terms of the precipitation deficit over an extended period of time. Agricultural drought results from a soil moisture deficit as consequence of the imbalance between water supply and evapotranspiration. Agricultural drought exists when root-zone water reserves are insufficient to sustain the plant demand. Hydrological droughts are related to the effects of rainfall deficit period on surface and subsurface water supply. Socioeconomic droughts are associated to the economic and social impacts as consequence of the extended periods of precipitation deficiency. The last type of drought may be considered a consequence of the others. The socioeconomic drought will not occur unless one or more of the other drought types take place.

Floods and droughts are extreme climatic events occurring at variable time frequencies in different areas of the world. Unlike floods, it is very difficult to determine the delimitation of the spatial extent of droughts. Likewise, drought's slow onset characteristics make it more difficult to recognize it until sometime has gone by. Thus, it is not easy to identify when drought starts and finishes. At present, there is not an objective and precise definition of drought. In a quest to compare drought measures from region to region or with past drought events, numerous specialized indices have been developed (Keyantash and Dracup 2002; Heim 2002). The meteorological indices measure the departures of precipitation that result

in water shortages or excesses using some criteria. A drought/excess would exist if the criteria defining the drought/excess were met and the index would then be a measure of the major drought/excess characteristics: duration, spatial extent, and intensity. Most indices have a fixed time scale, which does not allow identification of extreme deficits or excesses at shorter time scales. We mention in this paper three multiscale meteorological indices: the Statistical Z-score index (SZI), the China-Z Index (CHZI), and the well-known Standardized Precipitation Index (SPI).

If severe and extreme precipitation anomalies persist over long periods (longer than a season), they can affect large areas and cause tremendous social impact and important economic losses. This paper describes the main climatological aspects of water excesses and shortages in the La Plata Basin at different time scales in terms of a multiscale meteorological index.

2 Data and methodology

Precipitation data for the La Plata Basin come from the $0.5^\circ \times 0.5^\circ$ gridded data set CRU TS2.1 available at <http://www.cru.uea.ac.uk/>. A significant database of monthly rainfall time series (1,119 stations) for the region was collected, reformatted, and quality-checked during the Project “Assessing the Impact of Future Climatic Change on the Water Resources and the Hydrology of the Rio de La Plata Basin, Argentina, 1995–1999,” (Conway et al. 1999). The rainfall series were cross-checked with those in CRU global data set (Hulme 1994) and all the new stations were added to the global data set and new time series of gridded rainfall for 1901–1995 were constructed for the region (CRU TS 1.0: New et al. 2000). The grids were subsequently updated and extended to 2000 (CRU TS 2.0: Mitchell et al. 2004) and after that to 2002 (CRU TS 2.1: Mitchell and Jones 2005). The data set used contains monthly precipitation records from January 1901 to December 2002 (1,224 time points) for 2,043 grid points.

The well-known *SPI* index was originally proposed by McKee et al. (1993, 1995) to quantify the precipitation deficit on multiple time scales (3, 6, 12, 24, and 48 months), and the first application was to monitor droughts in Colorado State. To evaluate any drought or excess event, we need a specification of time scale since the event onset, duration, intensity, and ending are all dependent on time scale. The *SPI* is simply the transformation of the time series of 3, 6, 12, 24, and 48 months running precipitation totals into standardized normal distributions. This index is calculated by fitting a Gamma distribution function to the data, $G(x)$. Edwards and McKee (1997) suggest estimating the two parameters of the gamma function using the approximation of Thom (1958) for maximum likelihood method. Then, the

cumulative probability function is computed for an observed amount of precipitation occurring for a given month and time scale. Since the Gamma distribution, $G(x)$, is undefined for zero precipitation, $x=0$, we must do a simple transformation $H(x) = P(x = 0) + [1 - P(x = 0)] G(x)$, where $P(x=0) > 0$ is the probability of zero precipitation. Therefore, the cumulative probability distribution is then transformed into a standard normal distribution. An approximation to the inverse normal function provided by Abramowitz and Stegun (1965) is used to obtain the SPI value. SPI can monitor dry and wet periods over a wide spectrum of time scales (Hayes et al. 1999; Wu et al. 2001). A detailed description of SPI calculation can be found in Guttman (1999), Lloyd-Huges and Saunders (2002), or Western Regional Climate Center (2007), among others.

The SZI does not require adjusting the data to any specific distribution and can be calculated transforming the precipitation x_{ij} into typical standardized variables:

$$SZI[i](j) = \frac{x_{ij} - \bar{x}_i}{\sigma_i} \tag{1}$$

where i is the time scale of interest ($i=6, 9, 12,$ and 18 months), and j is the current month.

$$\bar{x}_i = \frac{1}{n} \sum_{j=1}^n x_{ij} \quad \text{and} \quad \sigma_i = \sqrt{\frac{1}{n} \sum_{j=1}^n (x_{ij} - \bar{x}_i)^2} \tag{2}$$

and n is the total number of months in the record.

The CHZI was introduced by the National Meteorological Centre of China (NMCC) in the 1990s; but, it is not easy to document the origin of such index. According to Wu et al. (2001), the CHZI is related to Wilson–Hilferty cube-root transformation, as a way to transform χ^2 -variables into the standard normal variates (Z-scores; Essenwanger 1976). The NMCC uses the CHZI only for 1-month time scale; but, Wu et al. (2001) have expanded the index to include multiple time scales. The CHZI is calculated as:

$$CHZI[i](j) = \frac{6}{\gamma_i} \sqrt{\frac{\gamma_i}{2} z_{ij} + 1} - \frac{6}{\gamma_i} + \frac{\gamma_i}{6} \tag{3}$$

where γ_i is the coefficient of skewness for the time scale i ($i=6, 9, 12,$ and 18 months) given by:

$$\gamma_i = \frac{\sum_{j=1}^n (x_{ij} - \bar{x}_i)^3}{n \sigma_i^3} \tag{4}$$

and j is the current month.

We transform monthly precipitation series, for each grid point, into precipitation index series at different time scales, $i=6, 9, 12,$ and 18 months using the CHZI, SZI, and the SPI. Therefore, we construct the time series $CHZI[i](t)$, $SZI[i](t)$, and $SPI[i](t)$ for $i=6, 9, 12,$ and 18 months. In order

to make a temporal intercomparison of the indices, the entire basin was divided in eight subregions and for each subregion the corresponding average precipitation index series, at different time scales, were calculated. For each index and time scale, the area-average time series were done as a simple average of all the grid points in the subregion. We did not apply any correction for latitude to the grid box areas. The cross-correlations between area-average indices were calculated in each subregion and evidenced a similar behavior for all indices. Cross-correlations between indices for the entire basin are listed in Table 2, where cross-correlations at the same temporal scales (diagonals) are indicated in boldface. The off-diagonal elements reveal a strong correlation between the indices at different time scales. Consequently, we prefer to use the *SPI* in our study of extreme events because it could be more familiar for the reader than the others. In Table 2, we can see that *SPI*[06] accounts for more than 70% of the *SPI*[09] variance, obtained by squaring the corresponding correlation value, and around 50% of *SPI*[12] variance and only 41% of the *SPI*[18] variance.

According to McKee et al. (1995) and Hayes et al. (1999), the drought and wetness intensity can be defined into different categories as shown in Table 3. The table also contains the corresponding probabilities of occurrence for each category. These probabilities of occurrence arise naturally from the normal probability density function. A water excess event implies severe or extreme wet condition, whereas, a water shortage event implies severe or extreme drought conditions.

The time structure of series was analyzed by means of a singular spectral analysis (SSA). SSA is a statistical method related to principal component analysis (PCA), but it is applied in the time domain. The objective is to describe the variability of a discrete and finite time series, in terms of its

Table 2 Cross-correlations between area-average *SPI*[i], *SZI*[i], and *CHZI*[i] ($i=6, 9, 12,$ and 18 months), for the whole basin

<i>SPI</i> [06]	<i>SPI</i> [09]	<i>SPI</i> [12]	<i>SPI</i> [18]	La Plata Basin
1	0.84	0.74	0.64	<i>SPI</i> [06]
	1	0.89	0.77	<i>SPI</i> [09]
		1	0.87	<i>SPI</i> [12]
			1	<i>SPI</i> [18]
0.99	0.84	0.77	0.64	<i>SZI</i> [06]
	0.99	0.89	0.77	<i>SZI</i> [09]
		0.99	0.87	<i>SZI</i> [12]
			0.99	<i>SZI</i> [18]
0.99	0.84	0.74	0.64	<i>CHZI</i> [06]
	0.99	0.89	0.77	<i>CHZI</i> [09]
		0.99	0.87	<i>CHZI</i> [12]
			0.99	<i>CHZI</i> [8]

Table 3 Classification scales for SPI used in this research and the corresponding event probabilities

Category		SPI value	Probability (%)
Extremely wet	Excess	2.00 or more	2.3
Severely wet		1.50 to 1.99	4.4
Moderately wet		1.00 to 1.49	9.2
Near normal		-0.99 to 0.99	68.2
Moderate drought		-1.00 to -1.49	9.2
Severe drought	Shortage	-1.50 to -1.99	4.4
Extreme drought		-2.00 or less	2.3

lagged autocovariance structure (Vautard and Ghill 1989; Ghill and Vautard 1991; Plaut and Vautard 1994; Vautard 1995). For a standardized time series $X(t_i)$ where the sample index i varies from 1 to N , and a maximum lag (or window length) is M , a Toeplitz-lagged correlation matrix is formed by

$$C_j = \frac{1}{N-j} \sum_{i=1}^{N-j} X(t_i)X(t_{i+j}) \quad 0 \leq j \leq M-1$$

The eigenvalue decomposition of the lagged autocorrelation matrix, C_j , produces temporal-empirical orthogonal functions *T-EOFs* (eigenvectors), and statistically independent temporal-principal components *T-PCs*, with no assumption as their functional form. Each component *T-PCs* has a variance λ_s (eigenvalue) and represents a filtered version of the original series, which can be classified essentially into nonlinear trends, deterministic quasi-oscillations, and noise. A significance test for the singular values, λ_s , can be made against a red noise null-hypothesis using a Monte Carlo method, generating an ensemble of 1,000 independent realizations (Allen and Smith 1996).

3 Trends over the La Plata Basin

We calculated for each index the corresponding mean regional series averaging monthly values over the entire basin ($SPI[i](t)$, $i=6, 9, 12$, and 18 months). Then, we analyzed the time structure of the series by mean of *SSA*, looking for

any possible low-frequency signal in $SPI[i](t)$ for the period 1901–2002. Table 4 shows the modes detected by *SSA* in the low-frequency band ($T > 10$ years) and the corresponding significance levels. In all the cases the first component, *T-PC1*, is associated with a nonlinear trend with different significance levels and explained variances. Figure 2 depicts $SPI[18](t)$ and $SPI[12](t)$ series and the corresponding partial reconstructions $RECPC1[18](t)$ and $RECPC1[12](t)$, based on *T-EOF1* and *T-PC1* for both series, corresponding to the nonlinear trends accounting for 22.4% and 18.3% of variance, respectively. The low-frequency behavior of averaged series $SPI[18](t)$, $SPI[12](t)$, $SPI[09](t)$, and $SPI[06](t)$ is associated with long-term changes in precipitation from the 1950 decade onwards, reported by several authors (Castañeda and Barros 1994; Minetti and Vargas 1998; Krepper and Sequeira 1998; Krepper and Garcia 2004) and the long-term response of the Paraná and Uruguay Rivers, as shown by other authors (Tucci and Clarke 1998; Krepper et al. 2003, 2008). Nevertheless, both nonlinear trends shown in Fig. 2 ($RECPC1[18](t)$ and $RECPC1[12](t)$) change recently. The increasing in precipitation show signs of stabilization during the last decade. Minetti et al. (2003) have studied nonlinear trends in annual precipitation over Argentina and Chile and they found large areas in Argentina with increasing trends after 1950 and a change in the slope during the last decade. As was mentioned in Section 1, this fact could be so important from the regional economy point of view. We cannot find other significant signals in averaged series $SPI[i](t)$, even in the interannual frequency band ($1 < T < 10$ years).

4 Climatological aspects of water excesses

Figure 3 show time series corresponding to the fraction of the total basin, experiencing water excess conditions, $SWET[i](t)$, at different time scales ($i=6, 9, 12$, and 18 months). The water excess condition is defined for each grid point according to Table 3 ($SPI[i](t) > 1.5$). Figure 3a–d shows outstanding excesses, associated to extreme precipitation during El Niño 1982–1983 for all time scales. In particular, at time scale of 18 months ($SWET[18](t)$), we can

Table 4 Leading modes detected by *SSA*, using a window length of 30 years, applied to $SPI[18]$, $SPI[12]$, $SPI[09]$ and $SPI[06]$ series

Mean regional series	Window lengths (months)	Components	Trend or dominant period (months)	Significance level (%)	Accounted variance (%)
$SPI[18]$	360	<i>T-PC1</i>	Nonlinear trend	26	22.4
$SPI[12]$	360	<i>T-PC1</i>	Nonlinear trend	12	18.3
$SPI[09]$	360	<i>T-PC1</i>	Nonlinear trend	6	15.4
$SPI[06]$	360	<i>T-PC1</i>	Nonlinear trend	2	11.4

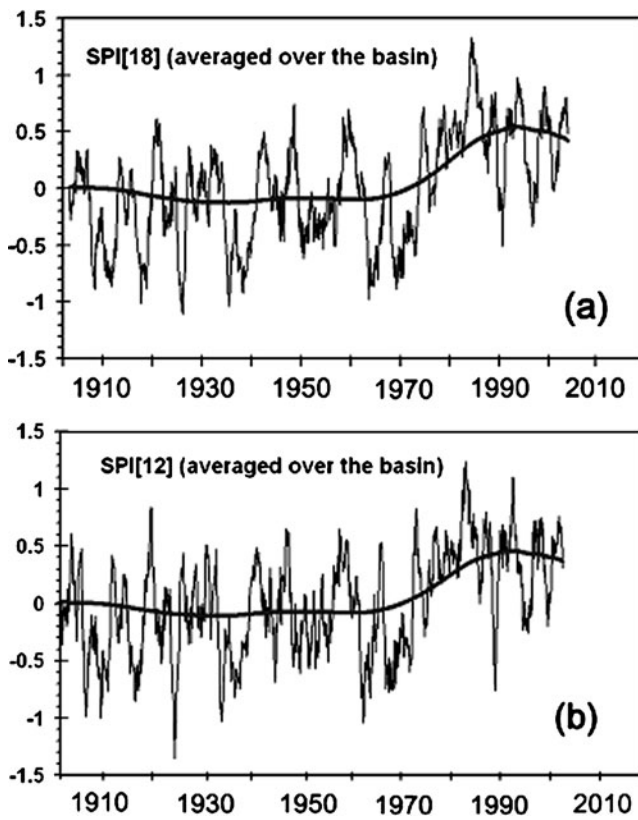


Fig. 2 a SPI[18] averaged over the entire basin and the corresponding RPC1[18] (solid line). b Idem for SPI[12]

appreciate from Fig. 3a that more than 48% of the total basin was affected by water excess conditions during July 1983.

The most obvious characteristic of Fig. 3 is that the behaviors of time series, $SWET[i](t)$, show a dependence on time scales. SSA was applied with different window lengths

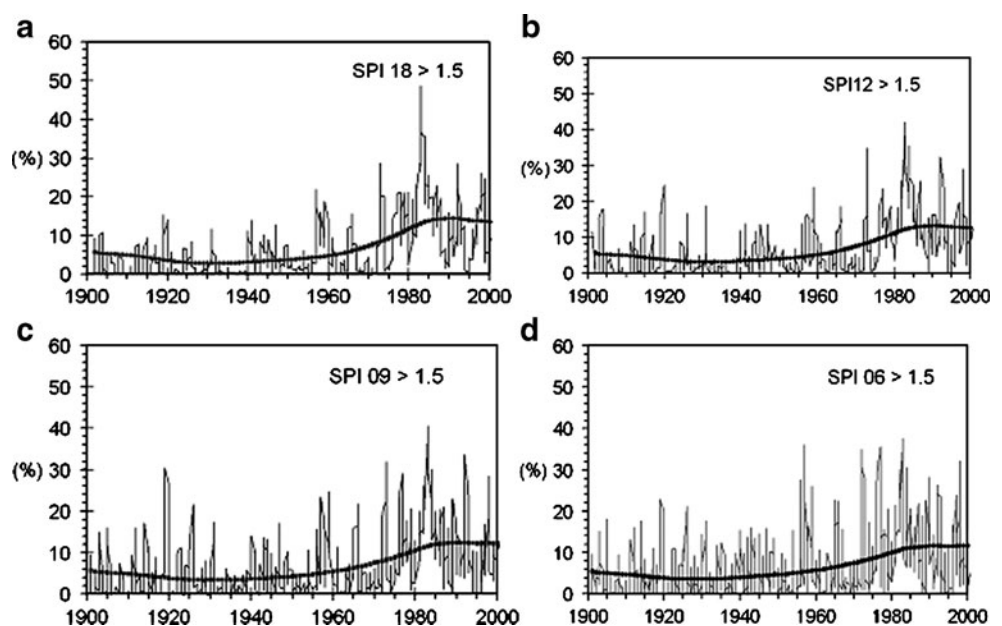
Table 5 Leading modes detected by SSA applied to $SWET[i](t)$ and $SDRY[i](t)$ for different time scales ($i=6, 9, 12, \text{ and } 18$ months)

Series	Window lengths (months)	Components (significance level <5%)	Dominant period (months)	Explained variance (%)
$SWET[18](t)$	360	T-PC1	Nonlinear trend	32.3
$SWET[12](t)$	360	T-PC1	Nonlinear trend	26.1
$SWET[09](t)$	360	T-PC1	Nonlinear trend	21.7
$SWET[06](t)$	360	T-PC1	Nonlinear trend	17.4

(M) to $SWET[i](t)$ series, in order to analyze the presence of any significant signal in LFB (trends or interdecadal quasi-oscillations). Table 5 summarizes the results for the different time series. All time series ($SWET[18](t)$ to $SWET[06](t)$) present significant positive trends with significance levels, lesser than >95%, after 1950s. Figure 3a shows $SWET[18](t)$ and the reconstructed time series $SPI18REC1(t)$, based on T-EOF1 and T-PC1. The reconstructed signal, $SPI18REC1(t)$, accounts for 32.3% of the total variance. Meanwhile, $SWET[12](t)$, $SWET[09](t)$, and $SWET[06](t)$, together with the corresponding reconstructed signals $SPI12REC1(t)$ (26.1%), $SPI09REC1(t)$ (21.7%), and $SPI06REC1(t)$ (17.4%), are shown in Fig. 3b, c, and d, respectively.

From the vulnerability point of view, the occurrences of situations with large portions of the entire basin under water excesses must be considered. A month when more than 30% of the total basin is under water excesses is defined as an excess critical month. In particular, we can appreciate in Fig. 3a that $SWET[18](t) > 30\%$ between March 1983 and

Fig. 3 Proportion of the La Plata basin experiencing water excesses for different time scales: a $SWET[18](t)$ and $SPI18REC1(t)$ (thick line); b $SWET[12](t)$ and $SPI12REC1(t)$ (thick line); c $SWET[09](t)$ and $SPI09REC1(t)$ (thick line); and d $SWET[06](t)$ and $SPI06REC1(t)$ (thick line)



May 1984; a period of fifteen excess critical months. This longest period was associated to the strong El Niño event of 1982–1983, and it produced the largest flood of the last century along the Paraná River. Nevertheless, not all the excess critical months were associated to SST warm events in the tropical Pacific Ocean. That is the case of excess critical months that took place in November 2001, February 2002, or June–July–August 2002. Figure 4 shows composite maps of the spatial distributions of SPI[18], SPI[12], SPI[09], and SPI[06] for critical months. Regions under water excesses in the composite maps (shaded areas in Fig. 4) correspond to the Upper Paraná and Uruguay basins. Table 6 shows the number of critical months for different periods (1901–2002, 1901–1950, and 1951–2002) at different time scales. We must note that the number of critical months increases with the time scale of the index and almost all the critical months occurred during the 1951–2002 period, as a consequence of low-frequency behavior of SWET[i](t) series.

4.1 Number and mean duration of water excess events

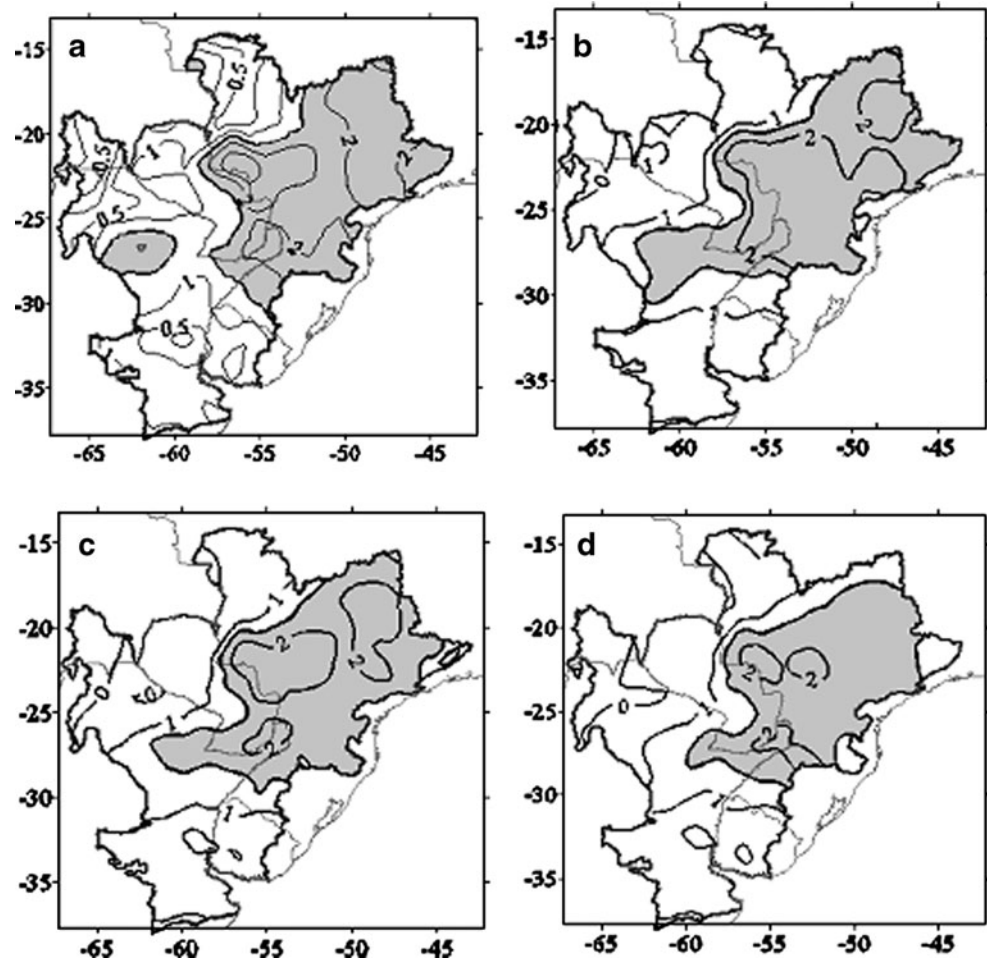
An event occurs when the index exceeds a given threshold. In particular, at a time scale of 18 months, an excess occurs

Table 6 Number of critical months with more than 30% of the La Plata basin experiencing excess conditions for different periods

(SPI[i]>1.5)	SPI[06]	SPI[09]	SPI[12]	SPI[18]
1901–2002	8	15	19	31
1901–1950	0	1	0	0
1951–2002	8	14	19	31

at month j , when $\text{SPI}[18](j) > 1.5$. Nevertheless, two consecutive months with $\text{SPI}[18](j) > 1.5$ and $\text{SPI}[18](j+1) > 1.5$ cannot be considered as two independent events; both months are part of the same excess event. Assuming in the SPI[18](j) time series an isolate interval of consecutive months with positive values, i.e., $\text{SPI}[18](j) > 0$ ($j = h, h+1, \dots, m$); preceded and followed by months with zero or negative values ($\text{SPI}[18](h-1) \leq 0$ and $\text{SPI}[18](m+1) \leq 0$). Furthermore, we assume that only some months in the interval $j = h, h+1, \dots, m$ satisfy the exceedance condition ($\text{SPI}[18] > 1.5$). All the consecutive months, $j = h, h+1, \dots, m$, belong to the same water excess event, bounded by the two zero crossings in the months $h-1$ and $m+1$ ($\text{SPI}[18](h-1) \leq 0$ and $\text{SPI}[18](m+1) \leq 0$).

Fig. 4 Composite maps of critical months with more than 30% of the entire basin experiencing water excesses: **a** SPI[18]; **b** SPI[12]; **c** SPI[09]; and **d** SPI[06]. Shaded regions indicate values of $\text{SPI}[i] > 1.5$ at different time scales



0), respectively. Therefore, individual events are defined by the zero crossings that bound the exceedance (Lloyd-Huges and Saunders 2002). The duration of an event is defined as the difference in months between two consecutive zero crossings which bound the exceedance. Figure 5 illustrates the number of water excess events ($SPI[i] > 1.5$) by grid cell across the La Plata Basin. Meanwhile, Fig. 6 shows the distribution of mean duration of excess events in months. The numbers of events, as well as their mean duration, have a strong dependence on the time scale.

In general, comparing Fig. 5 with Fig. 6, we can appreciate that there is a tendency (in all time scales) to relate regions, which experience water excesses more frequently with regions where the mean duration of said excesses is lower, and conversely. In other words, where excess events take place more frequently, their duration tends to be shorter, and conversely. Excess events classified as per $SPI[18]$ and $SPI[12]$ occur with high frequency over a large portion of the Upper Paraná basin (Fig. 5a and b). Meanwhile, the number of excess events for the shorter time scales ($SPI[09]$ and $SPI[06]$) presents isolated regions of relative maxima.

Table (7) lists the average number of excess events across the basin at different time scales for the periods 1901–2002, 1901–1950, and 1951–2002. Table (7b) and (c) list the mean duration (in months) and mean maximum duration of events, respectively, for the same periods. Single events that extended through the period 1950–1951

could be counted separately as two short events in the periods 1901–1950 and 1951–2002. In order to avoid such bias, we identify individual events by the zero crossing before the exceedance (the month the event started). Standard deviations are given between parentheses. The average number of excess events across the La Plata Basin, defined as per $SPI[18]$ and $SPI[12]$, is 5 ± 2 and 7 ± 3 , respectively, for the total period 1901–2002. The mean durations are 41 ± 15 months and 28 ± 7 months, respectively; whereas, the mean maximum durations for the same events and the same period are 68 ± 27 months and 51 ± 19 months.

In spite of the low-frequency behavior (positive trends) detected in $SPI[i]$ series (Section 3), Table 7 only shows a slight increase in the average number of excess events across the basin for the 1951–2002 period with respect to the 1901–1950 period. Nevertheless, if we compare mean duration and mean maximum duration of events (Table 7) between periods, we can observe that excess events occurring after 1950 tend to be longer than those that take place earlier.

5 Climatological aspects of water shortages

Figure 7 shows time series for the proportion of the La Plata Basin experiencing water shortages, $SDRY[i](t)$, as defined by $SPI[i] < -1.5$, at different time scales ($i=6, 9, 12$,

Fig. 5 Number of water excess events ($SPI[j] > 1.5$) by grid cell for the La Plata Basin (1901–2002): a $SPI[18]$; b $SPI[12]$; c $SPI[09]$; and d $SPI[06]$

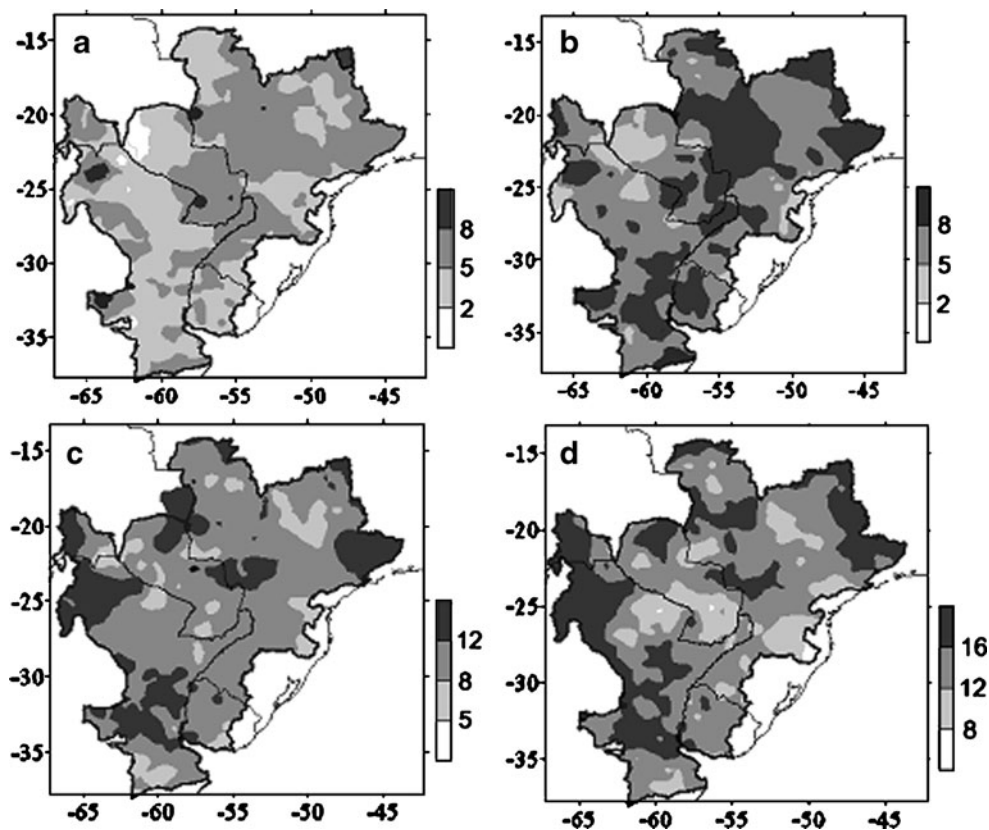
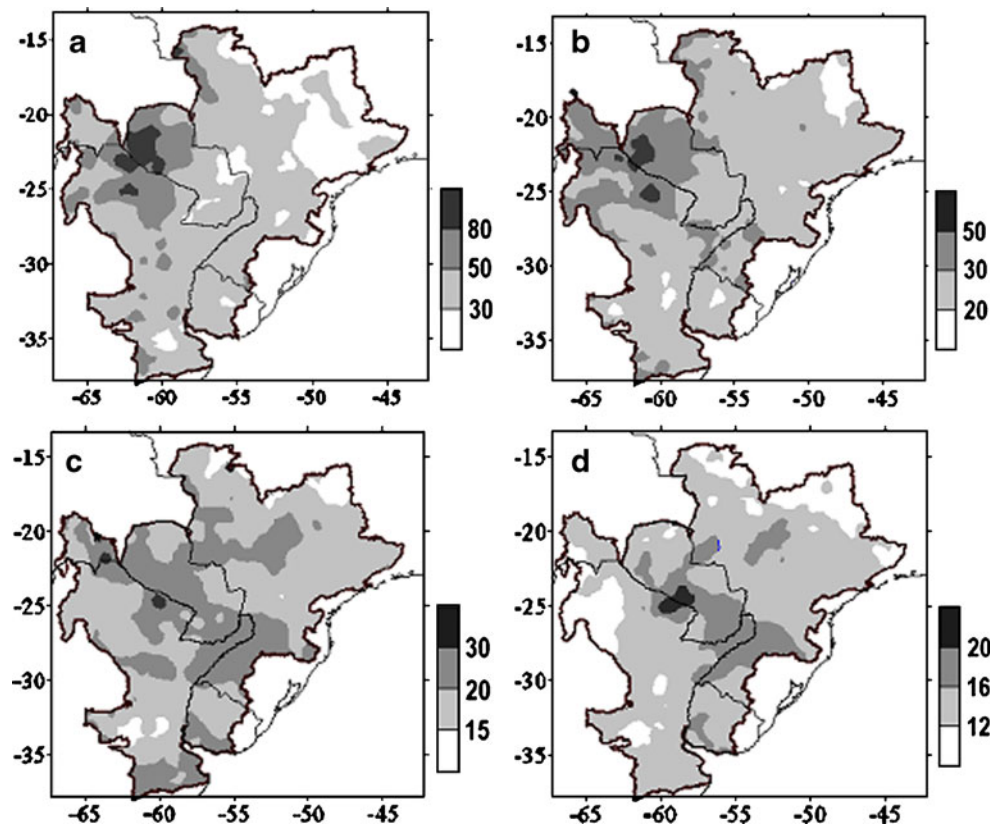


Fig. 6 Mean duration (in months) of excess events by grid cell for the La Plata Basin (1901–2002) at different time scales: **a** SPI[18], **b** SPI[12], **c** SPI[09], and **d** SPI[06]



and 18 months). We cannot find any significant low-frequency signals in $SDRY[i](t)$ series. From the vulnerability point of view, we must consider the occurrence of situations where large portions of the basin are affected by shortage conditions. An outstanding situation occurred between October 1924 and March 1925 (Fig. 7b), when a large portion of the basin, more than 50% of the total area, experienced water shortages at the 12 months time scales. Like in the case of water excesses, a month with more than 30% of the total basin experiencing water shortages conditions is defined as a shortage critical month. Not necessarily, the shortage critical months were associated to SST warm or cold events in the tropical Pacific Ocean. Figure 8 shows composite maps for shortage critical months at different time scales. An obvious characteristic of Fig. 7 is the dependence on time scale of $SDRY[i](t)$ series. The spatial distribution of regions under water shortages in the composite maps (shaded areas in Fig. 8a–d), depends on time scales, with a clear difference between intra-annual and longer time scales. At 18 and 12 months time scales, the critical regions cover a large portion of the basin, south to the 20° S; whereas, at shorter (intra-annual) time scales, the critical regions shift towards the northeast of the basin. Table 8 shows the number of shortage critical months for the period 1901–2002, 1901–1950, and 1951–2002. For

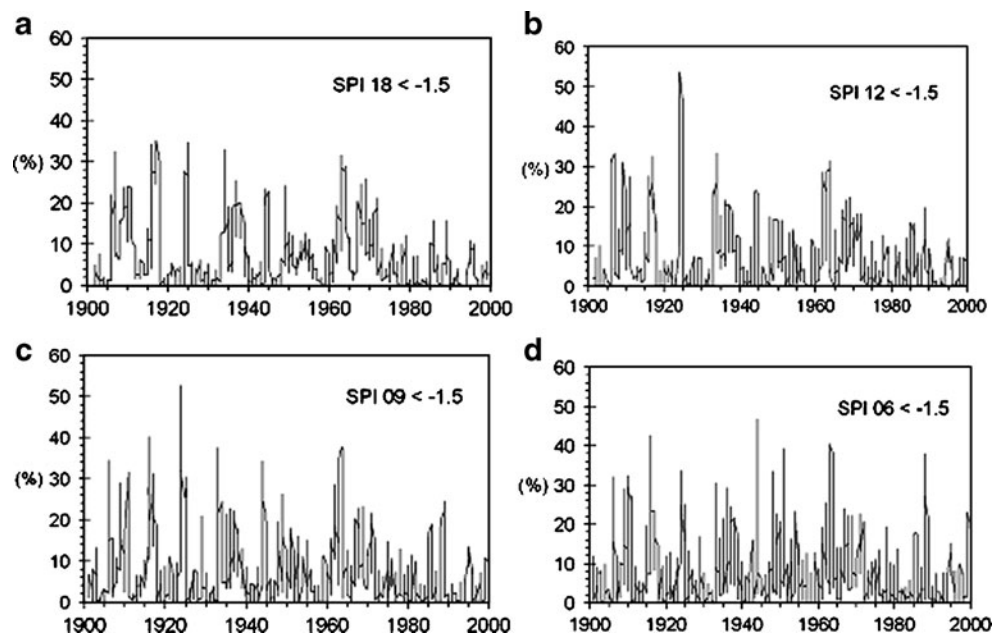
larger time scales (SPI[18] and SPI[12]), almost all the critical cases occurred in the period 1901–1950. However, for shorter time scales (SPI[09] and SPI[06]) some critical cases appeared in the period 1951–2002.

Table 7 Average number of excess events across the La Plata basin for 1901–2002, 1901–1950, and 1951–2002 periods, mean duration (in months) of excess events, and mean maximum duration (in months) of these events

	SPI[06]	SPI[09]	SPI[12]	SPI[18]
Average number of excess events across the La Plata Basin				
1901–2002	16 (± 4)	11 (± 3)	7 (± 2)	5 (± 2)
1901–1950	6 (± 3)	4 (± 2)	3 (± 2)	2 (± 1)
1951–2002	10 (± 2)	7 (± 2)	4 (± 1)	3 (± 1)
Mean duration (in months) of excess events				
1901–2002	13 (± 2)	19 (± 4)	28 (± 7)	41 (± 15)
1901–1950	13 (± 3)	17 (± 6)	21 (± 10)	26 (± 17)
1951–2002	14 (± 3)	21 (± 5)	31 (± 11)	45 (± 21)
Mean maximum duration (in months)				
1901–2002	28 (± 8)	38 (± 13)	51 (± 19)	68 (± 27)
1901–1950	20 (± 7)	25 (± 11)	28 (± 16)	32 (± 23)
1951–2002	26 (± 8)	36 (± 14)	49 (± 20)	65 (± 28)

Standard deviations are given in parentheses

Fig. 7 Proportion of the La Plata Basin experiencing shortages for different time scales: **a** SDRY[18](*t*), **b** SDRY[12](*t*), **c** SDRY[09](*t*), and **d** SDRY[06](*t*)



5.1 Number and duration of water shortage events

Figures 9 and 10 illustrate the number and mean duration (in months) of water shortage events ($SPI[i] < -1.5$) by grid cell across the La Plata Basin. If we compare Fig. 9 with Fig. 10,

we can appreciate (in all time scales) a strong relation between regions that experience shortage events more frequently with regions where the mean shortage duration is lower, and conversely. Thus, where shortage events are more frequent their duration tends to be shorter, and conversely.

Fig. 8 Composite maps of critical months with more than 30% of the entire basin, experiencing water shortage conditions: **a** SPI[18], **b** SPI[12], **c** SPI[09], and **d** SPI[06]. Shaded areas indicate values of $SPI[i] < -1.5$ at different time scales

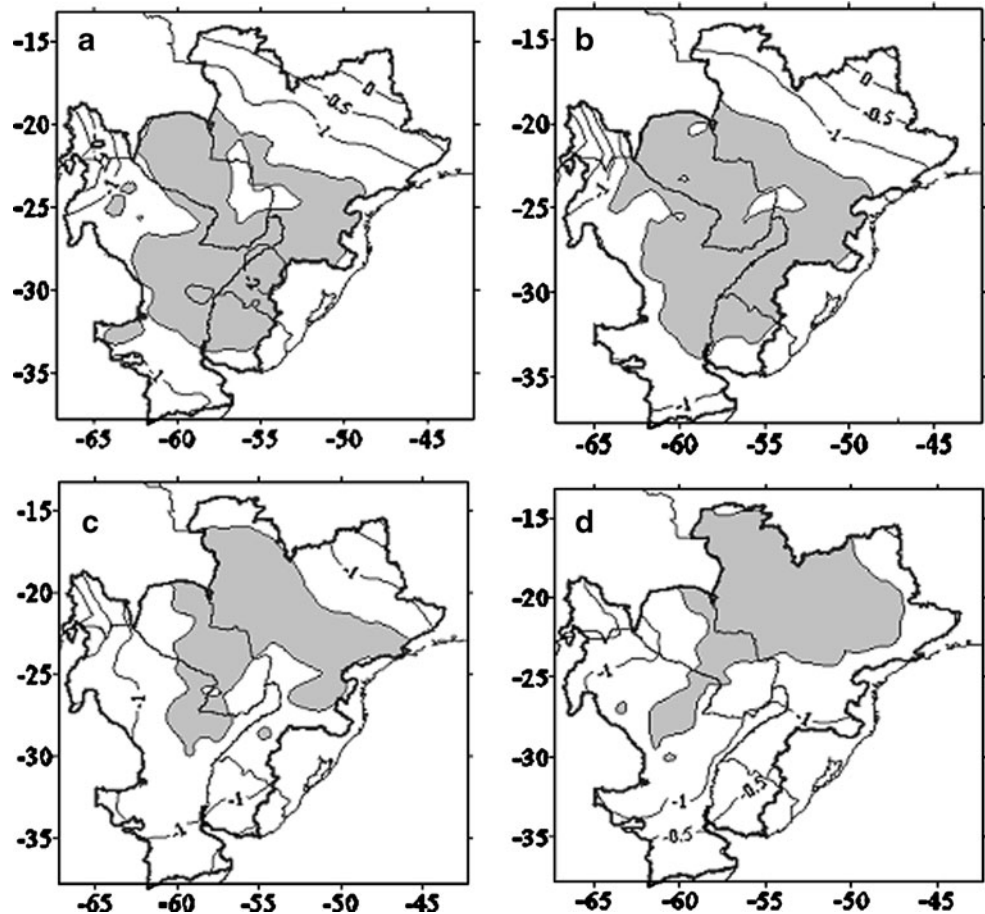


Table 8 Number of critical months with more than 30% of the La Plata basin experiencing shortage conditions for different periods

Water shortages (SPI[i] <-1.5)	SPI[06]	SPI[09]	SPI[12]	SPI[18]
1901–2002	17	17	15	15
1901–1950	12	14	14	14
1951–2002	5	3	1	1

Table 9a lists the average number of shortage events across the entire basin for the complete period 1901–2002 and two subperiods 1901–1950 and 1951–2002. Table 9b and c shows the mean duration and the mean maximum duration of these events for the same periods. The average number of shortage events across the La Plata Basin, as defined by SPI[18] and SPI[12], is 6 ± 2 and 8 ± 3 , respectively, for the total period 1901–2002. The mean durations are 43 ± 16 months and 28 ± 8 months, respectively; while, the mean maximum durations for the same events and the same period are 76 ± 31 months and 56 ± 24 months.

6 Summary and conclusions

We have presented a multitemporal climatology of water excess and shortage events, during the twentieth century, in

the La Plata Basin. The climatology is based on monthly SPI [i] calculated on a $0.5^\circ \times 0.5^\circ$ grid across the region at time scales of 6, 9, 12, and 18 months for the period 1901–2002. The use of SPI [i] facilitates the quantitative comparison of events at different locations and over different time scales.

The existence of precipitation trends was determined using mean regional series of average values over the entire basin (SPI [i], $i=18, 12, 9,$ and 6 months). SSA was applied to SPI [i] series looking for any low-frequency signal. In all the cases, the first temporal–principal component was associated with a positive nonlinear trend, showing a steady increase up until the 1980s when precipitation changes the slope during the last decade. As was mentioned in Section 1, this fact could be of great importance from the regional economy standpoint.

From the vulnerability point of view, we have analyzed the occurrence of critical months, with large portions of the total basin (more than 30%) experiencing excesses or shortage events by means of composite maps at different time scales. The excess regions (SPI [i] >1.5) in the composite maps of critical water excesses correspond to the Upper Paraná and Uruguay basins (shaded areas in Fig. 4), for all time scales. Meanwhile, the shortage regions (SPI [i] <-1.5) in composite maps of critical water shortages, depend on the index time scale. For SPI[18] and SPI[12], shortage regions correspond to large portions of the basin, between 20°S and 33°S

Fig. 9 Number of water shortage events (SPI [j] <-1.5) by grid cell for the La Plata Basin (1901–2002): a SPI[18], b SPI[12], c SPI[09], and d SPI[06]

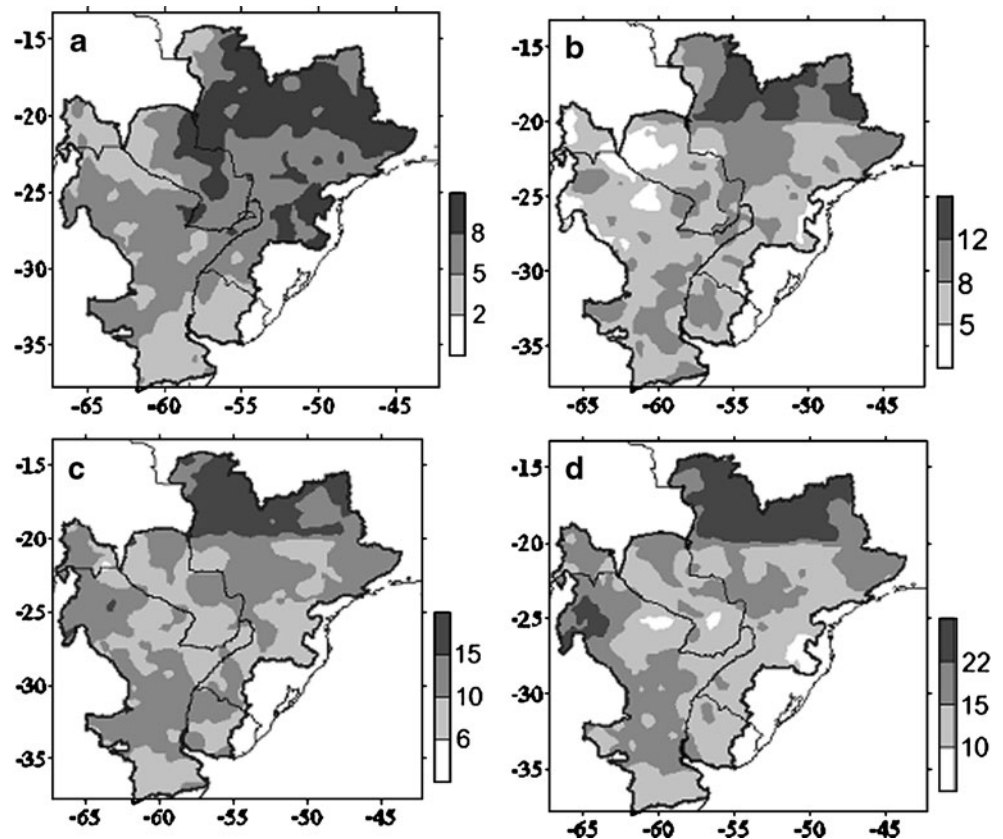
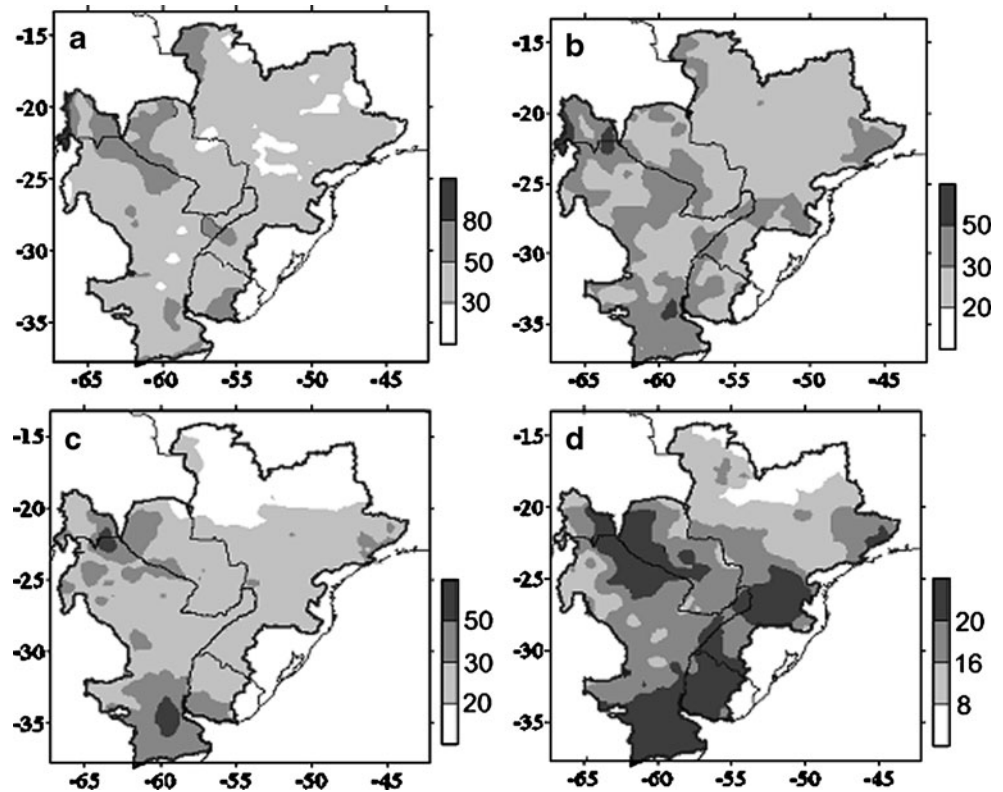


Fig. 10 Mean duration (in months) of water shortage events by grid cell for the La Plata Basin (1901–2002): **a** SPI [18], **b** SPI[12], **c** SPI[09], and **d** SPI[06]



(shaded areas in Fig. 6a and b). As regards interannual time scale (SPI[6] and SPI[9]), the shortage regions shift towards the northeast, covering the Upper basins of the Paraná and Uruguay rivers (shaded areas in Fig. 6c and d).

The number of excess critical months increases with the time scale of the index (Table 6), and almost all the excess critical months occurred in the period 1951–2002, as a consequence of the low-frequency precipitation behavior. That means a noticeable increase in the vulnerability to extended water excesses (more than 30% of the total basin, under water excess conditions) after 1950, especially over the Upper Paraná and Uruguay basins. The number of shortage critical months remains quite constant with time scale. On the other hand, at large time scale (SPI[18] and SPI[12]), almost all the shortage critical months occurred in the period 1901–1950 and only for interannual time scale (SPI[9] and SPI[6]), some critical months occurred after 1950. That means a noticeable decrease in the vulnerability of the basin to extended water shortages (more than 30% of the total basin, under water shortage conditions), as defined by SPI[18] and SPI[12], after 1950; and a moderate decrease in vulnerability to generalized shortages, as defined by SPI[09] and SPI[06], for the same period.

Individual shortage or excess events were defined by zero crossings that bound the exceedance ($SPI[i] < -1.5$ or $SPI[i] > 1.5$); and the duration of the event, as the difference in months between two consecutive zero crossings, which bound the exceedance. If we analyze the frequency and

mean duration of water excess events across the basin (Figs. 5 and 6), we can appreciate that there is a tendency to relate regions where excesses take place more frequently with regions where the mean duration of the events is lower, and conversely. As for the water shortage events, we can appreciate the same relationship, especially to the north of 20°S. Therefore, where shortage or excess events are

Table 9 Average number of shortage events across the La Plata basin for 1901–2002, 1901–1950 and 1951–2002 periods, mean duration (in months) of shortage events, and mean maximum duration (in months) of these events

	SPI[06]	SPI[09]	SPI[12]	SPI[18]
Average number of shortage events across the La Plata basin				
1901–2002	18 (±5)	12 (±4)	8 (±3)	6 (±2)
1901–1950	7 (±3)	5 (±2)	3 (±2)	3 (±1)
1951–2002	11 (±3)	7 (±2)	5 (±2)	3 (±2)
Mean duration (in months) of shortage events				
1901–2002	13 (±2)	19 (±4)	28 (±8)	43 (±16)
1901–1950	13 (±3)	17 (±6)	22 (±11)	43 (±17)
1951–2002	14 (±3)	21 (±6)	32 (±15)	39 (±29)
Mean maximum duration (in months)				
1901–2002	28 (±9)	40 (±14)	56 (±24)	76 (±31)
1901–1950	21 (±7)	25 (±11)	30 (±17)	61 (±28)
1951–2002	26 (±9)	38 (±15)	53 (±24)	52 (±35)

Standard deviations are given in parentheses

more frequent, their duration tends to be shorter, and conversely. If we compare the mean duration and maximum mean duration of water excess events for 1901–1950 and 1951–2002 periods, we can observe that excess events occurring after 1950 tended to be longer than those that had taken place before.

References

- Abramowitz M, Stegun I (1965) Handbook of mathematical functions with formulas, graphs and mathematical tables. Dover Publications Inc, New York
- Allen MR, Smith LA (1996) Monte Carlo SSA: detecting irregular oscillations in the presence of colored noise. *J Climate* 9:3373–3404
- Anderson RJ, da Franca Ribeiro dos Santos N, Diaz HF (1993) An analysis of flooding in the Paraná/Paraguay River Basin. LATEN Dissemination Note #5, The World Bank. Latin America & the Caribbean Technical Department, Environment Division
- American Meteorological Society (1997) Policy statement—meteorological drought. *Bull Amer Meteor Soc* 78:847–849
- Barros V, Silvestri G (2002) The relation between sea surface temperature at subtropical south-central Pacific and precipitation in Southeastern South America. *J Clim* 15:251–267
- Barros V, Doyle M, González M, Camilloni I, Bejarán R, Caffera RM (2002) Climate variability over subtropical South America and the South America monsoon: a review. *Meteorológica* 27(1–2):33–57
- Barros VR, Doyle ME, Camilloni IA (2008) Precipitation trends in southeastern South America: relationship with ENSO phases and with low-level circulation. *Theor Appl Climatol* 93:19–33
- Berberly EH, Barros VR (2002) The hydrological cycle of the La Plata basin in South America. *J Hydrometeor* 3:630–645
- Berberly HE, Doyle M, Barros V (2006) Regional precipitation trends. In: Barros V, Clarke R, Silva Diaz P (eds) *Climate Change in the La Plata Basin*. CONICET, Buenos Aires, pp 67–79
- Camilloni IA, Barros VR (2003) Extreme discharge events in the Paraná River and their climate forcing. *J Hydrol* 278:94–106
- Castañeda ME, Barros VR (1994) Las tendencias de la precipitación en el Cono Sur de América al este de los Andes. *Meteorológica* 19:23–32
- Castañeda ME, Barros VR (2001) Tendencias de la precipitación en el oeste de Argentina. *Meteorológica* 26:5–23
- Conway D, Jones PD, García NO, Vargas WM (1999) Assessing the impact of future climatic change on the water resources and the hydrology of the Río de La Plata basin, Argentina. Final report of work under contract ARG/B7-3011/94/25a. Commission of the European Communities. Buenos Aires, Argentina
- Diaz AF, Studzinski CD, Mechoso CR (1998) Relationship between precipitation anomalies in Uruguay and southern Brazil and Sea Surface Temperature in the Pacific and Atlantic Oceans. *J Climate* 11:251–271
- Doyle E, Barros VR (2002) Midsummer low-level circulation and precipitation in subtropical South America and related sea surface temperature anomalies in the South Atlantic. *J Climate* 15:3394–3410
- Dracup JA, Lee KS, Paulson EG (1980) On the definition of droughts. *Water Resour Res* 16:297–302
- Edwards DC, McKee TB (1997) Characteristics of 20th century drought in the United States at multiple timescales. Colorado State University, Fort Collins. *Climatology Report No. 97-2*, pp 155
- Essenwanger O (1976) Applied statistics in atmospheric science. Part A. Frequencies and curve fitting. Elsevier Scientific Publishing Company, Amsterdam
- García NO, Vargas WM (1996) The spatial variability of runoff and precipitation in the Río de la Plata Basin. *J Hydro Sci* 41:279–299
- García NO, Vargas WM (1998) The temporal climatic variability in the Río de la Plata Basin displayed by the river discharges. *Climatic Changes* 38:359–379
- Ghilm M, Vautard R (1991) Interdecadal oscillation and the warming trend in global temperature time series. *Nature* 359:324–327
- Giorgi F (2002) Variability and trends of sub-continental scale Surface Climate in the twentieth century. Part I: observations. *Clim Dyn* 18:675–691
- Grimm AM, Ferraz SET, Gomes J (1998) Precipitation anomalies in Southern Brazil associated with El Niño and La Niña events. *J Climate* 11:2863–2880
- Grimm AM, Barros V, Doyle M (2000) Climate variability in Southern South America associated with El Niño and La Niña events. *J Climate* 13:35–58
- Guttman NB (1999) Accepting the standardized precipitation index: a calculation algorithm. *J Am Water Resour Assoc* 35:311–322
- Hayes MJ, Svoboda MD, Wilhite DA, Vanyarkho OV (1999) Monitoring the 1996 drought using the standardized precipitation index. *Bull Amer Meteor Soc* 80:429–438
- Heim RR Jr (2002) A review of twentieth-century drought indices used in the United States. *Bull Amer Meteor Soc* 83:1149–1165
- Hulme M (1994) Validation of large-scale precipitation fields in global circulation models. In: Desbois M, Desalmand F (eds) *Global precipitation and climate change*. NATO ASI Series I, Vol. 26. Springer-Verlag, Berlin, pp 387–406
- Keyantash J, Dracup J (2002) The quantification of drought: an evaluation of drought indices. *Bull Amer Meteor Soc* 83:1167–1180
- Krepper CM, García NO (2004) Spatial and temporal structures of trends and interannual variability of precipitation over the La Plata Basin. *Quarterly International* 114:11–21
- Krepper CM, Sequeira ME (1998) Low-frequency variability of rainfall in Southeastern South America. *Theor Appl Climatol* 61:19–28
- Krepper CM, García NO, Jones PD (2003) Interannual variability in the Uruguay river basin. *Int J Clim* 23:1103–1115
- Krepper CM, García NO, Jones PD (2008) Low-frequency response of the Upper Paraná basin. *Int J Climatol* 28:351–360
- Labraga JC, Frumento O, López M (2000) The atmospheric water vapor cycle in South America and the tropospheric circulation. *J Climate* 13:1899–1915
- Lenters JD, Cook KH (1995) Simulation and diagnosis of the regional summertime precipitation climatology of South America. *J Climate* 8:2988–3005
- Liebmann B, Vera C, Carvalho LMV, Camilloni IA, Hoerling MP, Allured D, Barros VR, Báez J, Bidegain M (2004) An observed trend in central South America precipitation. *J Climate* 17:4357–4367
- Lloyd-Huges B, Saunders MA (2002) A drought climatology for Europe. *Int J Clim* 22:1571–1592
- McKee TB, Doesken NJ, Kleist J (1993) The relation of drought frequency and duration to time scales. *Proceeding of the Eight Conference on Applied Climatology*. 17–22 January, Anaheim, California. *Amer Meteor Soc. Boston, Massachusetts*, pp 179–184
- McKee TB, Doesken NJ, Kleist J (1995) Drought monitoring with multiple time scales. *Proceeding of the Ninth Conference on Applied Climatology*. 15–20 January, Dallas, Texas. *Amer Meteor Soc. Boston, Massachusetts*, pp 233–236
- Minetti JL, Vargas WM (1998) Trends and jump in the annual precipitation in South America, south of the 15°S. *Atmósfera* 11:205–221

- Minetti JL, Vargas WM, Poblete AG, Acuña LR, Casagrande G (2003) Non-linear trends and low-frequency oscillations in annual precipitation over Argentina and Chile, 1931–1999. *Atmósfera* 16:119–135
- Mitchell TD, Jones PD (2005) An improved method of constructing a database of monthly climate observations and associated high-resolution grids. *Int J Clim* 25:693–712
- Mitchell TD, Carter TR, Jones PD, Hulme M, New M (2004) A comprehensive set of high-resolution grids of monthly climate for Europe and the globe: the observed record (1921–2000) and 16 scenarios (2001–2010). *Tyndal Centre Working Paper* 55:25
- New M, Hulme M, Jones PD (2000) Representing twentieth century space–time climate variability. Part 2: Development of 1901–96 monthly grids of terrestrial surface climate. *J Climate* 113:2217–2238
- Nicolini M, Saulo AC, Torres JC, Saulo P (2002) Enhance precipitation over southeastern South America related to strong low-level jet events during austral warm season. *Meteorológica* 27:59–69
- Nogués-Paegle JN, Mo KC (1997) Alternating wet and dry conditions over South America during summer. *Mon Wea Rev* 3:279–191
- Nogues-Paegle J, Vera C (2009) South American precipitation regimes. IX International Conference on Southern Hemisphere Meteorology and Oceanography. 9 to 13 February 2009. Melbourne, Australia. http://www.bom.gov.au/events/9icshmo/manuscripts/TH0830_Paegle.pdf. Accessed July 2009
- Plaut G, Vautard R (1994) Spells of low-frequency oscillation and weather regimes in the Northern Hemisphere. *J Atmos Sci* 51:210–236
- Pisciottano G, Diaz A, Cazes G, Mechoso CR (1994) El Niño-Southern Oscillation Impact on Rainfall in Uruguay. *J Climate* 7:1286–1302
- Salio PV, Nicolini M, Saulo C (2002) Chaco low-level jet characterization during the austral summer season by ERA reanalysis. *JGR-Atmospheres* 107. doi:10.1029/2001JD001315
- Scian B, Labraga JC, Reimers W, Frumento O (2006) Characteristics of large-scale atmospheric circulation related to extreme monthly rainfall anomalies in the Pampa region, Argentina, under non-ENSO conditions. *Theor Appl Climatol* 85:89–106
- Thom HCS (1958) A note on the gamma distribution. *Mon Wea Rev* 86:117–122
- Tucci CEM (2001) Some scientific challenges in the development of South America's water resources. *J Hydrol Sci* 46:1–10
- Tucci CEM, Clarke RT (1998) Environmental issues in the La Plata basin. *Int J Water Resour Dev* 14:157–173
- UNESCO-WWAP (United Nations Educational, Scientific and Cultural Organization-World Water Assessment Program) 2007. The La Plata basin case study (Final Report), pp 516. http://www.unesco.org/water/wwap/case_studies/la_plata/151252e_rev.pdf Accessed in 2007
- Vautard R (1995) Patterns in time: SSA and MSSA. In: von Storch H, Navarra A (eds) Chapter 14 of analysis of climate variability: applications of statistical techniques. Springer Verlag, Berlin, p 327
- Vautard R, Ghil M (1989) Singular spectrum analysis in non-linear dynamics with applications to paleoclimatic time series. *Physica D* 35:395–424
- Vera C, Higgins W, Amador J, Ambrizzi T, Garreaud R, Gochis D, Gutzler D, Lettenmaier D, Marengo J, Mechoso CR, Nogues-Paegle J, Silva Dias PL, Zhang C (2006) Toward a unified view of the American monsoon systems. *J Climate* 19:4977–5000
- Wu H, Hayes MJ, Weiss A, Hu Q (2001) An evaluation of the standardized precipitation index, the China-Z and the statistical Z-score. *Int J Clim* 21:745–758
- Zhou J, Lau KM (1998) Does a monsoon climate exist over South America? *J Climate* 11:1020–1040